CFD Analysis of Off-design Centrifugal Compressor Operation and Performance

MingYao Ding
ANSYS, Inc.
Clinton Groth
University of Toronto Institute for Aerospace Studies
Suresh Kacker
Pratt and Whitney Canada
Douglas Roberts
Pratt and Whitney Canada

Abstract

This paper presents some of the results from a Master's thesis research into the performance and operation of a centrifugal compressor at off-design operating conditions using advanced computational fluid dynamics (CFD) techniques. ANSYS CFX is the CFD solver used in this blind study to evaluate the ability of modern CFD software to predict the performance of centrifugal compressors operating at highly complex flows regimes.

The off-design cases considered included compressor operations at 60%, 70%, 80%, 90%, 100% and 105% of the on-design rotational speed. Speed lines were generated for each case and compared to experimental measurements. The predicted results were found to match very closely with the experimental measurements.

The flow within the centrifugal compressor stage was also examined by considering various performance parameters and making use of three-dimensional flow visualizations. This allowed for a better understanding of the fluid behaviour within the centrifugal compressor.

Lastly, the benefits of unsteady (time accurate) simulation on centrifugal compressor performance predictions were investigated. The results obtained showed that unsteady simulations noticeably improve the accuracy of the compressor performance predictions.

Introduction

This paper describes an effort to investigate and better define the capabilities of a modern CFD solver in predicting the off-design performance of centrifugal compressors. The results will validate the use of commercially available CFD software tools for these problems and lead to a better understanding of the flow phenomenon within the centrifugal compressor. Furthermore, better compressor designs that enhance off-design operation and improve performance could result once confidence is gained in applying CFD analysis tools to the centrifugal compressor design process.

The centrifugal compressor stage considered in this study was designed by Pratt and Whitney Canada. It employs a tandem split impeller with a pipe diffuser configuration [8] as shown in Figure 1.

The compressor geometry was provided in CATIA format, ANSYS ICEMCFD was used to generate the appropriate mesh, and ANSYS CFX was used to solve the off-design compressor flow problem. The entire range of off-design conditions were investigated and compared to experimental data. Furthermore the effects of different mesh densities and turbulence models were also examined. Finally the flow characteristics were examined to identify and quantify the sources of losses and inefficiencies.

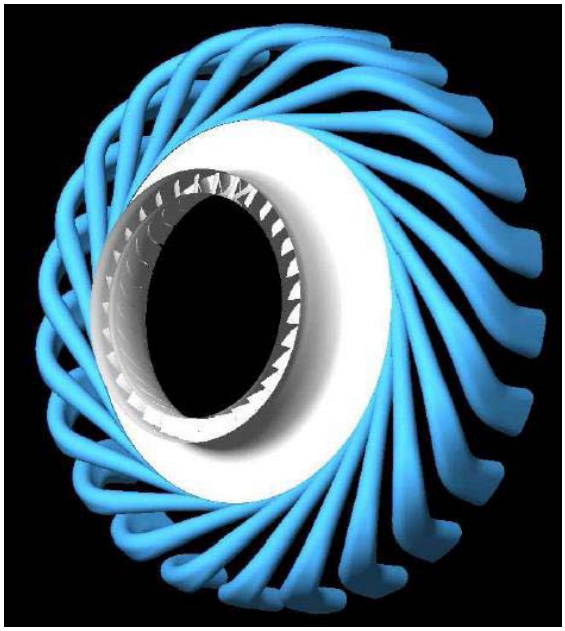

Figure 1. Pratt and Whitney Canada Centrifugal Compressor

Motivations

Centrifugal compressors are vital to many mechanical systems. The focus of this thesis is on these types of machines as applied to gas-turbine engines. This particular application places very strict requirements on weight, efficiency and operating flexibility, which has led to arguably the most advanced and high performance compressor designs. As the performance boundaries are pushed ever higher and efficiencies are further increased, the task of designing better and better compressors becomes more difficult. However some additional improvements are still possible through a better understanding of the flow behaviour over the entire operational range. This can be best accomplished using high-fidelity computational fluid dynamics modelling.

Currently centrifugal compressors are designed for optimal operations at a single speed - the design speed. The design speed is usually set at the point where the compressor will operate for the longest duration, such as the cruising speed for turbo-fan aircraft engines. However, compressors must also operate at speeds other than the design point for various amounts of time. A low efficiency at these off-design points can lead to problematic engine starts and poor performance during acceleration. Furthermore, as the compressor becomes more optimized for the design speed, it is becomes increasingly likely that this effort can adversely affect its performance at off-design conditions.

Mathematical modelling and Numerical Solution Procedure

In order to accurately simulate the internal fluid flow within a centrifugal compressor, the Favre-averaged Navier Stokes equations were solved using commercial software. Furthermore, commercially available mesh generation and computer aided design (CAD) programs were used to define the geometry and grid for the problem. This section will briefly review some of the mathematical modelling and numerical solution procedures.

Navier-Stokes Equations

The fundamental equations that describe fluid flow behaviour are the Navier-Stokes equations. This is a set of five (two scalar and 1 vector) partial differential equations that describe the conservation of mass, momentum and energy. The integral form of the Navier-Stokes equations is as follows.

$$\frac{\partial}{\partial t}\int_v \rho dv + \int_S \rho U_j dn_j = 0$$
$$\frac{\partial}{\partial t}\int_v \rho U_i dv + \int_S \rho U_j U_i dn_j = -\int_S P dn_j + \int_S \mu_{eff}\left(\frac{\partial U_i}{\partial x_j} + \frac{\partial U_j}{\partial x_i}\right) dn_j + \int_v S_{Ui} dv$$
$$\frac{\partial}{\partial t}\int_v \rho\phi dv + \int_S \rho U_j \phi dn_j = \int_S \Gamma_{eff}\left(\frac{\partial \phi}{\partial x_j}\right) dn_j + \int_v S_\phi dv$$

where ρ is the density, v is the volume, U_i is the velocity component, dn_j are elemental surface area, μ_{eff} is the effective coefficient of viscosity, S_{Ui} is a momentum source term, φ is the internal energy per unit mass, Γ_{eff} is the effective net heat flux and S_φ is the energy source term.

Turbulence modelling

Turbulent flows occur at high Reynolds numbers, when the inertia of the fluid overwhelms the viscosity of the fluid, causing the laminar flow motions to become unstable. Under these conditions, the flow is characterized by rapid fluctuations in pressure and velocity which are inherently three dimensional and unsteady. Turbulent flow is composed of large eddies that migrate across the flow generating smaller eddies as they go. These smaller eddies in turn generates smaller eddies until they become small enough that their energy is dissipated due to the presence of molecular viscosity.

The full influence of the turbulent fluctuations on the mean flow must be modelled. In order to use a larger mesh size and still capture the turbulent flow, the Favre averaged Navier-Stokes equations are used [16]. The Favre averaged Navier-Stokes equations are

$$\frac{\partial \bar{\rho}}{\partial t} + \frac{\partial}{\partial x_i}\left(\bar{\rho}\tilde{u}_i\right) = 0$$
$$\frac{\partial}{\partial t}\left(\bar{\rho}\tilde{u}_i\right) + \frac{\partial}{\partial x_j}\left(\bar{\rho}\tilde{u}_i\tilde{u}_j\right) = -\frac{\partial P}{\partial x_i} + \frac{\partial}{\partial x_j}\left(\bar{t}_{ji} - \overline{\rho u_j'' u_i''}\right)$$
$$\frac{\partial}{\partial t}\left[\bar{\rho}\left(\tilde{e} + \frac{\tilde{u}_i\tilde{u}_i}{2}\right) + \frac{\overline{\rho u_j'' u_i''}}{2}\right] + \frac{\partial}{\partial x_j}\left[\bar{\rho}\tilde{u}_j\left(\tilde{h} + \frac{\tilde{u}_i\tilde{u}_i}{2}\right) + \tilde{u}_j\frac{\overline{\rho u_j'' u_i''}}{2}\right] =$$
$$\frac{\partial}{\partial x_j}\left[-q_{Lj} - \overline{\rho u_j'' h''} + \overline{t_{ji}u_i''} - \overline{\rho u_j''\tfrac{1}{2}u_i''u_i''}\right] + \frac{\partial}{\partial x_j}\left[\tilde{u}_i\left(\bar{t}_{ij}\right) - \overline{\rho u_i'' u_j''}\right]$$

where here, $\widetilde{u}_i$ is the averaged velocity and $u_i^{"}$ is the fluctuations due to turbulence. It is assumed that $u_i = \widetilde{u}_i + u_i^{"}$. The variable t_{ji} is the instantaneous viscous stress tensor, h is the specific enthalpy, and q_{Li} is the laminar mean heat-flux vector.

The Favre averaging of the Navier -Stokes equations introduces higher-order velocity correlations that reflect the influence of the turbulence on the mean flow. The Favre averaged Reynolds stress tensor is related to the time-averaged product of the turbulent velocity fluctuations and is given by $\bar{\rho}\tau_{ij} = -\overline{\rho u_i'' u_j''}$.

The Reynolds stress tensor is generally not known and a closure model is required to relate this tensor to the mean flow fields. Most turbulence models provide a method for calculating the Reynolds stress tensor. One way of doing this involves the use of the Boussinesq eddy-viscosity approximation. This approximation assumes that the Reynolds stress tensor is a product of the turbulent eddy viscosity, υ_T, and the mean strain-rate tensor, S_{ij}. The general form of the Boussinesq eddy-viscosity approximation is

$$\tau_{ij} = 2\nu_T S_{ij} - \frac{2}{3}k\delta_{ij}$$

and the specification of the eddy viscosity becomes the focus of the turbulence modelling.

Procedure

A step-by-step approach was adopted for this study. First the impeller section was simulated and a comprehensive mesh-density study and turbulence model study was conducted to determine the magnitude of the possible errors involved due to these numerical techniques. Then the entire centrifugal compressor stage was simulated at the design speed. Various simulation parameters were fine tuned in order to match the experimental setup as accurately as possible and to increase numerical convergence speed. Finally, the off-design study was conducted for a range of operating points from of 60% to 105% of design speed. The results were compared to experimental measurements, and analyzed to better understand the flow physics at off-design operating conditions.

CAD Geometry Definition

CAD geometries for this study were generated in CATIA. CATIA at its core is a full functioned CAD solid modelling tool that is widely used in the aerospace industry. This CAD tool was used for this thesis to define the geometries for the compressor stage as shown in Figure 2. A key benefit of CATIA is that it integrates smoothly with ANSYS ICEMCFD which allows for the complex geometries generated in CATIA to be easily and reliably imported into ANSYS ICEMCFD

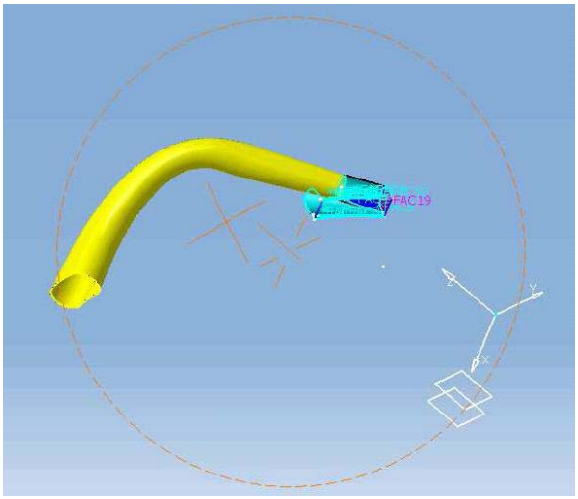

Figure 2. Diffuser geometry in CATIA

Mesh Generation

Mesh generation was performed using ANSYS ICEMCFD. This program was chosen because it is full featured and it is compatible with a wide range of CAD and commercial computational fluid dynamics software.

With ANSYS ICEMCFD, it is possible to import CAD geometry and generate both structured and unstructured meshes based on it. For this thesis, the computational domain contains two different meshes; the impeller section consisted of structured hexahedral meshes as shown in Figure 3 while the diffuser section was meshed using unstructured tetrahedral mesh as shown in Figure 4.

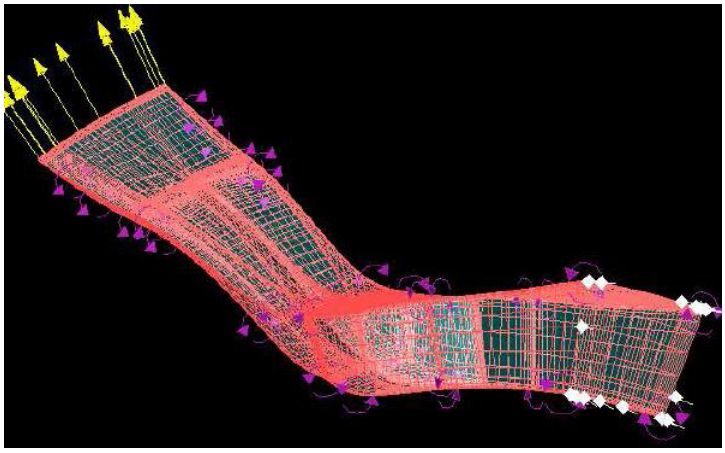

Figure 3. Impeller mesh.

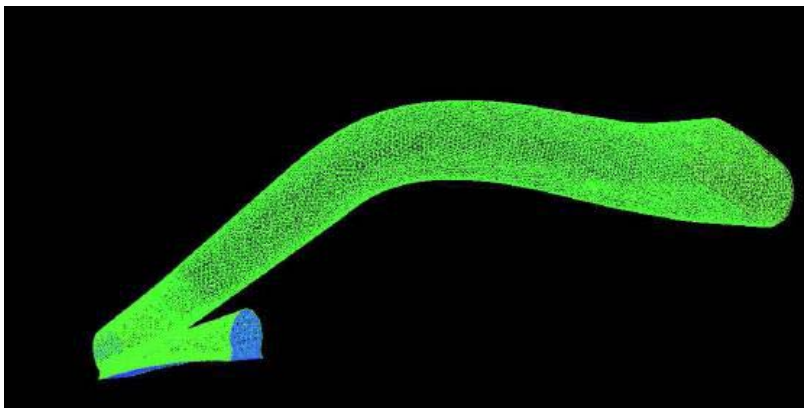

Figure 4. Diffuser mesh.

The ANSYS ICEM CFD hexahedral mesh generator is an object-based, semi-automatic, multi-block structured or unstructured, surface and volume mesh generator. The block topology model is generated directly on, but independent of, the underlying CAD geometry. It is recognized as one of the fastest commercially available hexahedral mesh generation tools. ANSYS ICEMCFD is projection based in that the surfaces of the mesh are automatically projected on to the nearest CAD surface. It is also possible to specify the projection of points, edges and surfaces for a greater degree of control.

The ANSYS ICEMCFD tetrahedral mesh generator automatically generates tetrahedrals in a 3D space enclosed by an assembly of CAD surfaces. The resulting tetrahedral mesh is independent of the underlying CAD structure. Once the CAD geometry is imported, a tetrahedral mesh can be generated within a volume enclosed by three dimensional surfaces. In addition, it is possible to specify curves and points to control the mesh in area that are not smooth. Element sizes on surface, curves, points and density volumes are defined to control the mesh density and size. The unstructured mesh is generated automatically and it is possible to smooth and refine the mesh afterward. The prism layers are generated after the tetrahedrals are created by building prisms from the triangular surface mesh. Prism layers are used along the wall surfaces to resolve the boundary layers.

CFX Flow Solver

The computational fluid dynamics solver used in this thesis was ANSYS CFX. CFX is a technology leader, providing highly accurate results, robust solutions and industry-leading parallel efficiency. CFX was chosen because it represented a state of the art commercial CFD solver package able to tackle the complex problems faced in this thesis. Furthermore, our partners at Pratt and Whitney Canada expressed an interest in evaluating the ability of CFX to predict off-design centrifugal compressor performance. A summary of various aspects and properties of the ANSYS CFX flow solver can be found in its online documentation.

Domain Interface

Due to their complex geometry, centrifugal compressors can be difficult systems to analyze using CFD. The configurations considered in this thesis consisted of a fast rotating impeller attached to a stationary pipe diffuser. In order to simulate the entire compressor stage, the two sections (rotating impeller and stationary diffuser) must be modelled together. To reduce computational cost, only a single passage is considered as part of the computational domain for both the impeller and the diffuser and the off-design simulation was modelled as a steady state problem.

The two sections of the compressor were meshed separately; the impeller was meshed with structured hexahedral while the diffuser was meshed with unstructured tetrahedrals with prism layers to resolve the boundary layer. Each mesh is designated as a distinct domain and the two are connected at the interface. CFX offers three ways of handling the passing of the solution content across the domain interfaces between the rotor and the diffuser. First is the frozen rotor approach where the frame of reference is changed according to the motions defined for the domain, but the relative orientation of the geometry is fixed. The second method is called the stage averaging. Here circumferential averaging is applied at the interface between the rotating and the stationary domains. This method helps in the convergence of a steady state simulation because the interface solution state is circumferentially uniform. A one-time mixing loss is added by the stage averaging at the interface. This model accounts for the time averaged interaction effect but neglects the transient interaction effect. The last method is the transient rotor-stator simulation. This is used for fully unsteady simulations to take into account the true transient interactions of the flow between the domains. The main disadvantage of this method is the high cost of the simulations in terms of CPU time and disk space requirements.

To decrease the computational resource cost, the stage averaging technique is used almost exclusively here to solve the off-design centrifugal compressor stage problem. However the mixing plane averaging can result in errors in the simulation result and numerically difficulties in some cases. This led to the use of the frozen rotor interface and the transient simulations to gauge the benefits of these techniques.

Analysis

The primary goal of this research is to assess the current capabilities of CFD analysis tools to predict flows within centrifugal compressors across a wide range of off-design operating conditions. Following the on-design analysis of the impeller, the problem of the simulation of the entire compressor stage under various operating conditions was tackled. The predicted results were compared to off-design performance data provided by Pratt & Whitney Canada. Engineers from Pratt & Whitney Canada were very helpful in specifying and explaining the experimental setup which ensured that the experimental configurations of the compressor were accurately modelled.

Simulation setup

The simulation setup for the compressor stage analysis is as follows. First the CAD geometries were generated in CATIA. Two separate geometries were needed, one for the impeller and a second for the diffuser. This was necessary because the diffuser is physically separate from the impeller and they move at different rotational velocities. To model the relative motions of the impeller and diffuser, each section was meshed independently and defined as a separate computational domain in the CFD solver, and an interface surface was defined to connect them.

The on-design operating conditions was computed first and mesh density and turbulence model studies were conducted to assess mesh requirements for the stage. After the on-design results were deemed satisfactory, five off-design cases were studied.

In order to remove the effect of differing inlet temperature associated with the experimental measurements, a corrected rotational velocity [10] was used in place of the actual mechanical rotational speed. The corrected rotational velocity for the CFD simulation was matched to that of the experimental, and since the inlet boundary conditions for the simulations were kept constant, an associated physical rotational velocity was calculated for the CFD simulation based on the corrected rotational velocity and the inlet boundary conditions.

The initial conditions within the compressor are estimated automatically by CFX based on the boundary conditions. However when the compressor was simulated at operating conditions, the numerical solution was found to diverge. Therefore, a rotational velocity ramping function was used at start up.

The impeller rotational velocity at start up was set such that the initial velocity is about 25% of the desired velocity and it was increased to the desired velocity over the next 75 iterations. This allows the flow to develop at slower rotational velocities such that when the desired rotational velocity is reached, the flow properties within the compressor are much closer to the desired steady-state solution. This technique generates improved estimates for the initial data, which was necessary because of the aggressive time steps (1/rotational velocity) used in order to quickly reach convergence. As a comparison, this time step is over 10 times larger than the one automatically estimated by CFX based on mesh dimensions.

The Mesh

Two meshes were needed for the compressor stage simulation. The impeller mesh is a structured multi-block hexahedral mesh divided into 48 blocks. The diffuser was meshed with an unstructured tetrahedral mesh was used with 10 prism layers along the wall surfaces to resolve the near-wall boundary layer flow. The mesh was refined to better resolve the flow in the knife edge area and any non-smooth areas.

Because of the large number of simulations needed for the off-design performance comparison, the mesh size must be kept small in order to complete the simulations in a reasonable amount of time. However a coarser mesh could negatively affect the accuracy of the results. Therefore a mesh density study was conducted to gauge the amount of mesh dependent error for mesh sizes in the range of 1.6 to 3.2 million nodes. It was found that the resulting difference between the mesh sizes investigated was in general no more than 0.5% for the variables of interest. Therefore the mesh used in the simulation contained a total of 1.6 million nodes.

Boundary Conditions

As mentioned above, the stage simulation is composed of two sections - impeller and diffuser - connected by a ``stage type'' mixing plane where the flow properties are averaged circumferentially. The exit of the impeller and the inlet of the diffuser make up this interface. At the inlet, the boundary was defined as a subsonic inlet, with measured total temperature, total pressure and flow direction profiles. The turbulence level was defined to be medium intensity of about 5%. Periodic boundary conditions were applied to the impeller periodic plane at the middle of the impeller flow passage. The blades, hub and shroud were defined as adiabatic walls with the appropriate rotational velocity. Figure 5 provides a summary of the boundary conditions used in the centrifugal compressor stage simulations.

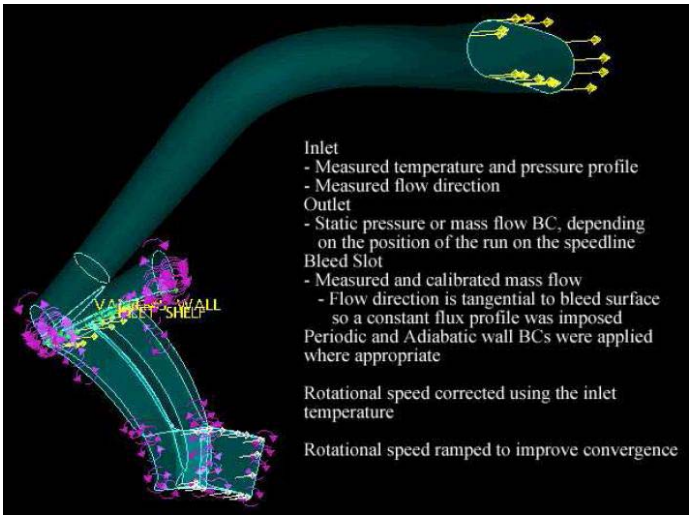

Figure 5. Compressor stage boundary conditions.

A bleed slot was specified on the impeller hub at the mixing plane. The bleed slot was added because it is physically impossible to attach a rapidly rotating impeller to a stationary diffuser therefore a gap exists between the two sections as shown on Figure 6. High pressured gas escapes through this gap and it has been shown to noticeably affect compressor performance. In the experiment, the bleed flow was controlled carefully to be a fixed fraction of the total inlet flow and this was the way it was specified in the simulation. Because the primary flow is generally tangential to the surface of the bleed slot boundary, a simple uniform flow profile normal to the surface was specified to better insure convergence of the simulations.

Boundary conditions for the diffuser are comparatively simpler. The inlet to the diffuser section was taken to be the second surface for the mixing plane interface boundary. The two open surfaces of vaneless section were specified to be periodic boundaries. The solid surfaces of the diffuser were specified to be adiabatic wall boundaries. At the exit plane, a subsonic outlet boundary condition was imposed with either the mass flow rate or the static pressure specified. A mass flow rate boundary condition is used for compressor simulation cases near surge. This is because near surge, the pressure difference remains constant even though the mass flow rate changes. On the other hand, the static pressure boundary condition is used for simulation cases near choke because during choke, the mass flow rates through the compressor remains constant while the pressure ratio changes.

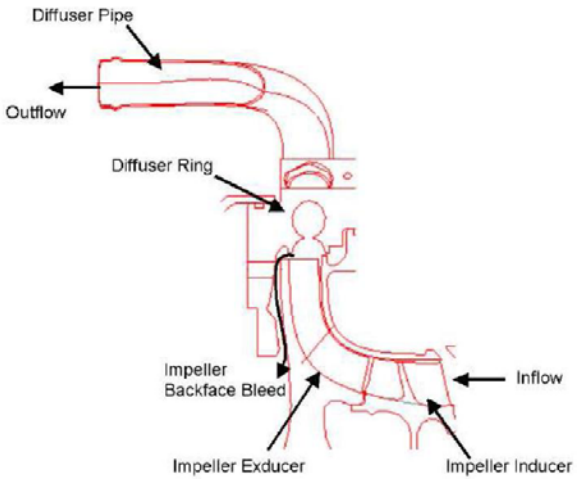

Figure 6. Compressor stage schematic diagram [9]

Analysis Results & Discussion

Simulation of the off-design performance of the centrifugal compressor stage was considered for six off-design speeds (RPMs): 60%, 70%, 80%, 90%, 100% and 105% of design speed. Six different performance speed lines were constructed for these off-design operating conditions. These numerical predictions of the speed lines are compared directly to available experimental data. These results will be presented in this section.

Comparison of Performance Predictions to Experimental Measurements

The first performance measure investigated was the total to static pressure ratio. This is a ratio of the static pressure ratio at the exit divided by the total pressure at the inlet. Figure 7 and Figure 8 shows the plots of total to static pressure ratio as a function of the inlet corrected and exit corrected mass flow. The plot of the normalized pressure ratio as a function of mass flow is called the speed line. The plots clearly show the stall, operating and choke regions of the speed lines. The blue asterisks represent the experimental results while the solid lines represent the CFD predictions for each rotational velocity. Because surge is an unsteady phenomenon that cannot be modelled with a steady state simulation, the convergence rate for the calculations tends to stall near surge. Although the results do not diverge, the solutions oscillate, which generates a high degree of error. The location where residual stalling first appears is shown on the graphs as "x". Any decrease in mass flow rates after these points will result in greater and greater oscillations in the computed solution and the solution residual measures.

The experimental data was gathered until surge becomes evident, therefore for each experimental speed line for which there is data, the lowest mass flow rate can be considered to represent the onset of surge. However the experimental determination of the onset of surge can be a challenging task. Mild surge can develop in a subtle manner where small regions/cells of reverse/recirculating flow reside in the compressor unnoticed with very little effect on the overall compressor performance. As the mass flow rate is lowered these regions/cells will become more prominent until the surge cycle suddenly causes noticeable reverse flow through the entire compressor stage. Therefore the actual measured surge locations are usually at a lower mass flow rate than the actual onset of unsteady surging effects. These unsteady effects can have a very significant effect and cannot be accounted for in the steady-state compressor simulations.

The plots of the pressure ratio versus inlet corrected mass flow of Figure 7 are in a format most commonly adopted to indicate centrifugal compressor performance. This graph shows clearly the pressure increase at each mass flow rate and rotational velocity setting, as well as the choke and surge regions of the performance envelope. The graph also shows that overall, the CFD simulation results is in good agreement with the experimental results. At low rotational velocities, the flow rate simulation matched the experiment very closely, as the rotational velocity increased, error increased in that the mass flow rates are over predicted. In general the shape of the predicted curves matches the experimental measurements very well. The choke and the operating regions are very clearly characterized. The surge region curves are not as smooth because the unsteady nature of the flow in this region is not conducive to numerical convergence and the numerical results were found to fluctuate. The locations for residual stall show that as the rotational velocity is decreased, more and more of the speed-line experiences convergence difficulties. These results were still plotted on the graph because the solution often matched the experimental data very well even-though convergence difficulties were experienced.

The plots of the pressure ratio versus inlet flow rate show that the mass flow rate was over-predicted for higher operational speeds. At 100% operating speed, the mass flow rate over prediction was about 1.7% as shown on Figure 7. This error becomes steadily smaller until it becomes almost non-existent at 60% rpm. This is probably due to the higher rotational velocities causing greater separation of the boundary layers and other turbulent flow features that are not captured accurately by a two equation turbulence model.

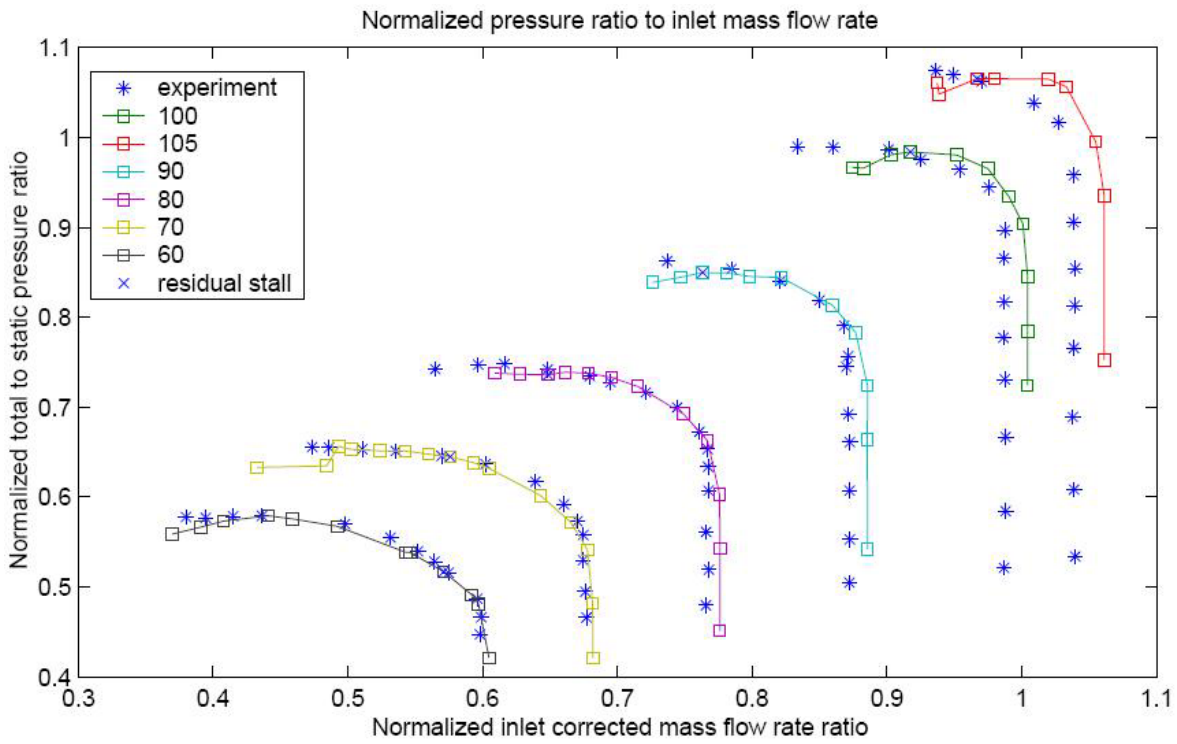

Figure 7. Normalized pressure ratio to inlet mass flow rate

The plots of the pressure ratio versus exit corrected mass flow rate shown in Figure 8 are useful in understanding compressor off-design operation. The exit corrected mass flow rate graph is useful because for jet engines, the goal of the compressor is to supply a steady flow of air into the combustion section. This means that the running line or operating points of the gas turbine is fixed to a constant corrected exit mass flow rate. In plots of performance variable versus the exit corrected mass flow, the operating points appear as a vertical (constant mass flow) line. This ensures that the combustors always get the same corrected mass flow rate at all rotational velocities. The mass flow rate at the diffuser exit is 97.4% the value at the inlet because 1.6% is removed at the bleed slot. However this does not result in a simple shift of the pressure ratio to inlet corrected mass flow rate graph because of the temperature and pressure corrections. When the mass flow rate is corrected by the diffuser exit values, the corrected mass flow rates are lowered and spread out. In the choke region, the absolute mass flow rate stays constant as shown in the inlet corrected flow graphs. However the exit pressure changes which cause the exit corrected mass flow rate to vary. This effect slowly diminishes until surge where the pressure changes become very small.

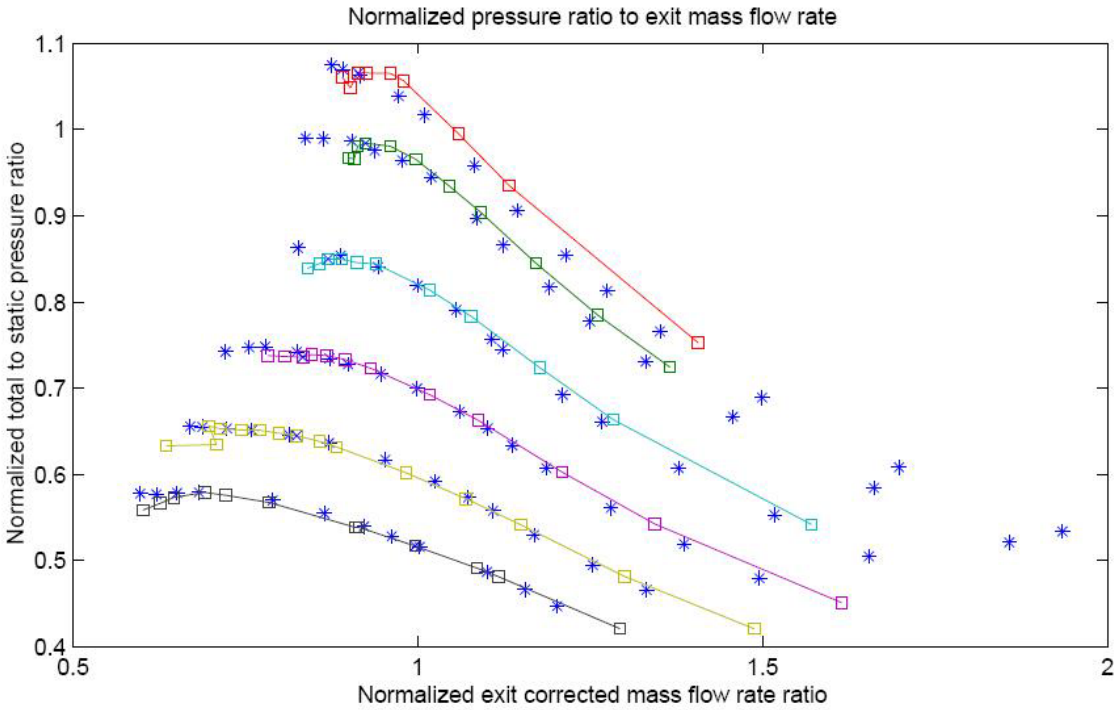

Figure 8. Normalized pressure ratio to exit mass flow rate

One crucial value gained from the speed-lines for design purposes is the surge margin. This is the distance between the operating point and the surge location on the speed-line graph. Because strong compressor surge can be catastrophic to gas turbine operation, it is essential to set the operating point away from surge so that minor flow variations does not cause surge to occur. This means the operating point of the compressor is set at a higher mass flow rate than value associated with the maximum pressure ratio because the mass flow rate at maximum pressure ratio point is considered to represent the beginning of the surge region. To specify the surge margin at the design stage requires the ability to predict the onset of surge. Figure 9 and Figure 10 summarizes the predictions of surge obtained from the current simulations. The graph plots the difference between the predicted surge points to the experimentally measured point and is presented as a percentage of the experimentally measured mass flow rate at surge. It should be noted that the experimental measurement of surge using the pressure ratio measurement alone is not extremely accurate and a significant amount of error can exist in the measured values. The graph shows two lines, the upper error limit shows the location of the maximum pressure ratio in the simulated data set and the lower error limit shows the value of the following point with a lower mass flow rate. The experimentally determined surge location was set as the first point following the highest pressure ratio point, or the value with the lowest mass flow rate value if the measured curve has no positive slope. The upper and lower error limit shows that the error of the simulated surge location is between the two curves. The curves show an upward trend with respect to the rotational velocity. A linear fit of the upper error limit curve shows that the simulation error increases by about 1.5% for each 10% increase in the rotational velocity.

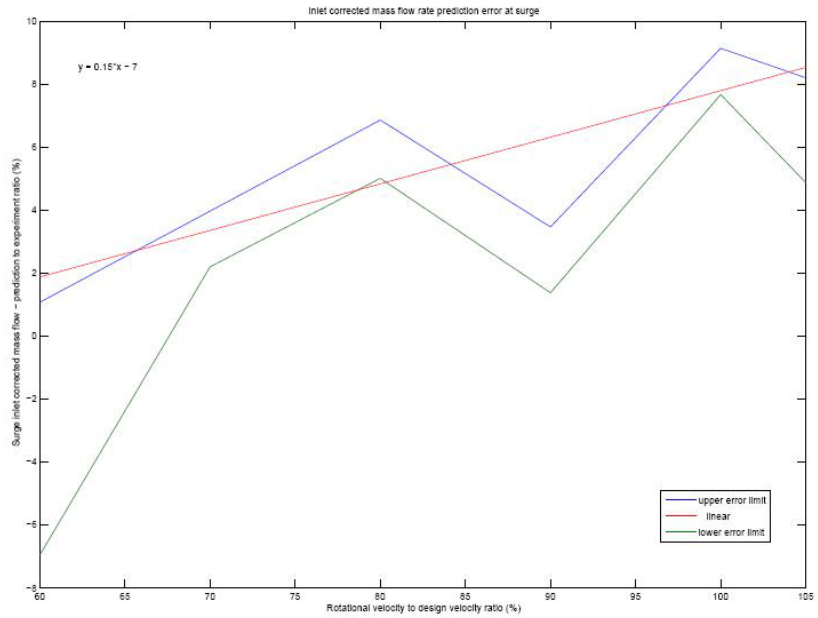

Figure 9. Inlet corrected mass flow rate prediction error at surge

The difference between the predicted mass flow rate at choke and the experimental measurements is shown in Figure 10. Since for each rotational speed, the mass flow rate in the choke region is constant with varying pressure ratio, it is easy to compare the differences between the simulated solutions and the experimental results. This graph shows that the error increases as the rotational velocity increases. Since mass flow rate is constant for compressors in choke, the values for both the simulation and the experiment are taken at the lowest pressure ratio for each speed-line. The blue line shows the difference between the simulation and the experiment while the red line shows a linear fit of the values. The linear fit shows that the error increases at about 0.24% per 10% increase in the rotational velocity.

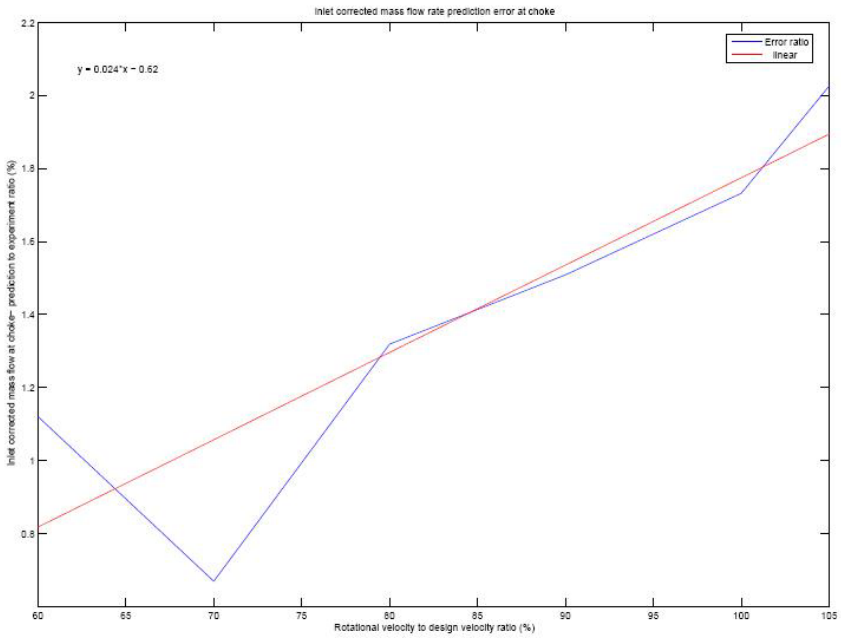

Figure 10. Inlet corrected mass flow rate prediction error at choke

Unsteady Analysis

Much of the physical modelling error in the computed solution and numerical difficulties in obtaining the steady state CFD simulations for the centrifugal compressor may be attributed to the use of the mixing plane averaging at the impeller-diffuser interface. Therefore it is likely that by eliminating the use of the mixing plane and solving the centrifugal compressor problem as a fully unsteady problem, more accurate results may be obtained. The main disadvantage is the fact that unsteady simulations are far more computationally expensive, making an extensive off-design study impractical as part of this study. It is felt that future work is needed in this area.

Solving the centrifugal compressor problem as an unsteady simulation using the commercial CFD flow solver requires a number of changes to the problem definition. First the geometry of computational section must be adjusted to minimize the area difference at the interface between the impeller and the diffuser. Because there are 31 impeller passages and 22 diffuser passages the single passage computational geometry used in the steady state simulations had an area difference of more than 40%. This means that the area of the diffuser at the impeller-diffuser interface is 40% greater than the area of the impeller. In the unsteady simulation this is not acceptable because of the significant circumferential variations in the flow at the interface. The ideal setup would be to simulate the entire compressor, but this was judged to be too costly for the computational resources available. Instead the computational domain was defined to include three impeller and two diffuser passages which resulted in an area difference of 6.45%. The CFX solver stretches the solution at the interface during the calculations to remove the area difference and allow the simulation to converge, but this obviously introduces some modelling errors.

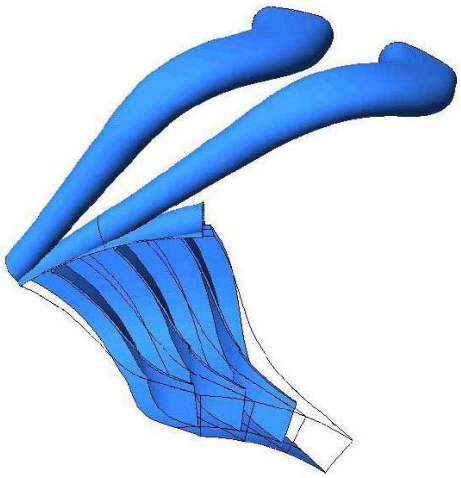

Figure 11. Unsteady simulation geometry

The geometry for the unsteady simulation is as shown in Figure 11, depicting the three impeller passages and two diffuser passages. Each flow passage was defined to be a separate domain. The three impeller domains were connected by setting the interfaces between the domains to be fluid-fluid interfaces. Periodic boundary conditions are then applied to the two outer boundary surfaces that represent the middle of the gas passage between the blades. This attempt to simulate the entire impeller disk based on the three passages modelled. The two diffuser passages are connected in a similar manner.

Because the impeller rotates at a very high speed, the time step for the unsteady simulation was set at 10^{-5}s. This time-step was chosen so that the impeller moves about one degree after each time-step. Each simulation was run for 900 iterations (which represents 2.5 revolutions of the impeller wheel) to reach a quasi-steady state solution. The initial condition is estimated using the steady state result from a CFD run of the unsteady geometry with the ``frozen rotor'' interface. Two turbulence models were investigated, the SST and stress-ω models. However, due to the computational cost of the unsteady simulation, only five

runs were completed during the time available for this thesis work. The results of the simulations are shown in Figure 12.

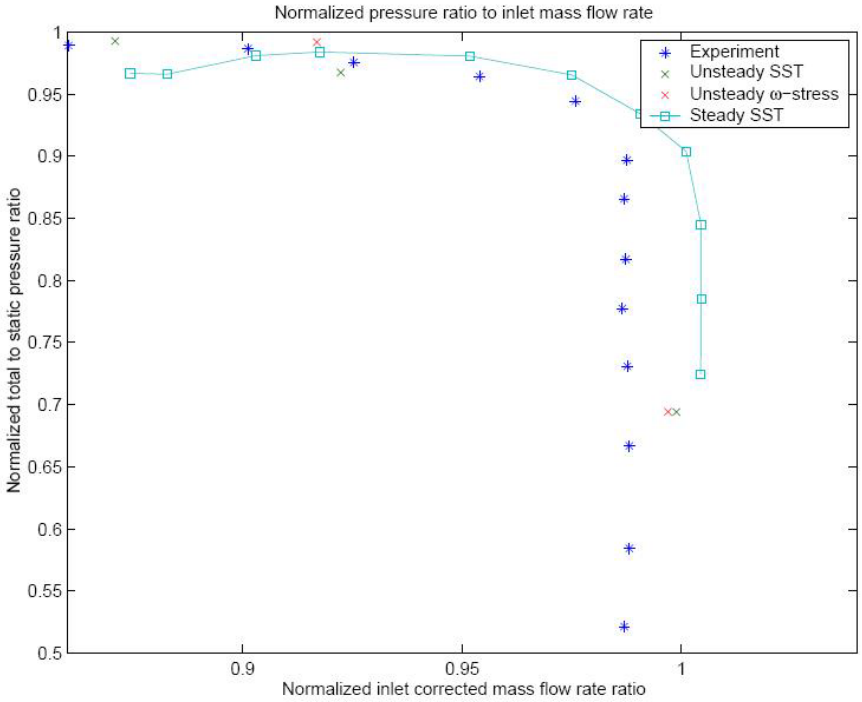

Figure 12. Normalized pressure ratio to inlet mass flow rate

Although the unsteady simulations are somewhat limited and do not cover the entire operation envelope, they do show considerable promise. The mass flow prediction error at choke is reduced to less that 1% for both turbulence models in the unsteady simulations. The SST model has an error of 0.76% and the stress-ω model has an error of 0.65% both well below the estimated 1% experimental error. The limited number of simulation results makes it difficult to determine the location for the onset of surge. However at low mass flow rates, the unsteady simulation seems to be more accurate than the steady state simulations. In particular at 0.87 normalized inlet-corrected mass flow rate, while the steady state simulation incorrectly predicted that the flow is clearly in surge, the unsteady simulation result was very close to that of the experiment. The difference between the results of the SST and the stress-ω model is somewhat inconclusive because of the limited number of unsteady simulations that were carried out

Examining the qualitative aspects of the unsteady flow solutions shows that there are significant circumferential variations at the mixing plane. Furthermore, the difference in the pitch area between the impeller and diffuser results in additional unsteady flow patterns. These can be seen in Figure 13 and Figure 14 in which the flow profiles for the total pressure at choke and Mach number during surge are shown respectively at the impeller-diffuser interface.

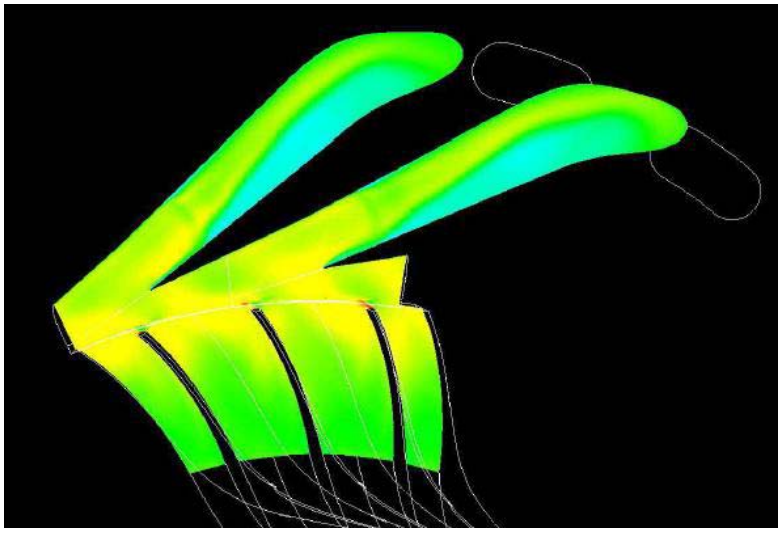

Figure 13. Total pressure plot at choke

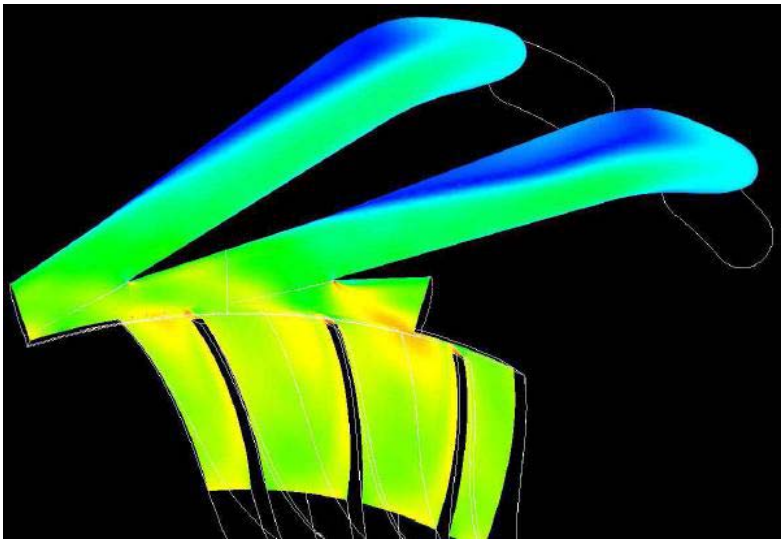

Figure 14. Mach number plot at surge

Conclusion

The main contribution of this thesis was to demonstrate that off-design performance of a centrifugal compressor can be accurately simulated using commercial CFD software, with CATIA as the CAD package, ANSYS ICEMCFD to generate high quality meshes and CFX as the CFD solver. Entire speed maps can be generated with high accuracy, particularly for lower rotational velocities. However, modelling the off-design centrifugal compressor as a steady state problem with a mixing plane interface does pose a problem for very low rotational velocities where the unsteady phenomena are more prominent and the mixing plane assumption less valid. Surge prediction is also an unsteady phenomenon which means it is an area that can be improved upon. The results of the unsteady centrifugal compressor computations indicate that fully unsteady flow analyses can yield better performance predictions particularly at high rotational speeds.

Overall this thesis was very successful in achieving the aim of validating commercial CFD software for the prediction of complex off-design centrifugal compressor performance and to gain a better understanding of the centrifugal compressor physics.

References

1. T. J. Barth and D. C. Jespersen. The design and application of upwind schemes on unstructured meshes. Paper 89-0366, AIAA, January 1989.
2. W.P. Jones and B.E. Launder. The prediction of laminarization with a two-equation model of turbulence. International Journal of Heat and Mass Transfer, 15:301{314, 1972.
3. L.M. Larosiliere, J.R. Wood, M.D. Hathaway, A.J. Medd, and T.Q. Dang. Aerodynamic design study of advanced multistage axial compressor. Paper TP2002-211568, NASA, December 2002.
4. B.E. Launder, G.J. Reece, and W. Rodi. Progress in the development of a Reynolds-stress turbulence closure. Journal of Fluid Mechanics, 68:537-566, 1975.
5. F. R. Menter. Improved two-equation k - ω turbulence models for aerodynamic flows. Reference Publication 103975, NASA, 1992.
6. F. R. Menter. Two-equation eddy-viscosity turbulence models for engineering applications. AIAA Journal, 32(8):1598{1605, August 1994.
7. B. S. PETUKHOV and L.I. ROIZEN. Generalized relationships for heat transfer in a turbulent flow of gas in tubes of annular section. HIGH TEMPERATURE, 2:65-68, 1964.
8. D. A. Roberts and S. C. Kacker. Numerical investigation of tandem-impeller designs for a gas turbine compressor. Report 2001-GT-324, Pratt and Whitney Canada for ASME, 2001.
9. D. A. Roberts and R. Steed. A comparison of steady-state centrifugal stage CFD analysis to experimental rig data. Submitted to the 2004 ANSYS CFX conference, 2004.
10. D. G. Shepherd. Principles of Turbomachinery. The Macmillan Company, New York, 1956.
11. G.J. Skoch, P.S. Prahst, M.P. Wernet, J.R. Wood, and A.J. Strazisarl. Laser anemometer measurements of the flow field in a 4:1 pressure ratio centrifugal impeller. Report ARLTR-1448, NASA and Army Research Laboratory, March 1997.
12. P. R. Spalart and S. R. Allmaras. A one-equation turbulence model for aerodynamic flows. Paper 92-0439, AIAA, January 1992.
13. C. G. Speziale, R. Abid, and E. C. Anderson. A critical evaluation of two-equation models for near wall turbulence. Technical report, ICASE, June 1990.
14. D. E. van Zante, A. J. Strazisar, J.R. Wood, M.D. Hathaway, and T.D. Okiishi. Recommendations for achieving accurate numerical simulation of tip clearance flows in transonic compressor rotors. Paper TM2000-210347, NASA, September 2000.
15. M.P. Wernet, M.M. Bright, and G.J. Skoch. An investigation of surge in a high-speed centrifugal compressor using digital PIV. Paper TM2002-211832, NASA, December 2002.
16. D. C. Wilcox. Turbulence Modeling for CFD. DCW Industries, Canada, 1993.